TITLE: The TrkB agonist 7,8-dihydroxyflavone changes the structural dynamics of neocortical pyramidal neurons and improves object recognition in mice

AUTHORS: Marta Perez-Rando[1#*], Esther Castillo-Gomez[1,2,4 # *], Clara Bueno-Fernandez[1], Juan Nacher [1,2,3, *]

[1]. Neurobiology Unit, Program in Neurosciences and Interdisciplinary Research Structure for Biotechnology and Biomedicine (BIOTECMED), Universitat de València, Burjassot, Spain

[2]. CIBERSAM: Spanish National Network for Research in Mental Health, Spain

[3]. Fundación Investigación Hospital Clínico de Valencia, INCLIVA, Valencia, Spain

[4]. Current address: Department of Medicine, School of Medical Sciences, Universitat Jaume I, Castellón de la Plana, Spain

[#]. Both authors have contributed equally to this work.

*. Corresponding authors: Dr. Juan Nacher (Neurobiology Unit. Cell Biology Dpt. Interdisciplinary Research Structure for Biotechnology and Biomedicine (BIOTECMED). Universitat de València. Dr. Moliner, 50. Burjassot, 46100. Spain. Telf: (+34) 963543241. e-mail: nacher@uv.es) & Dr. Esther Castillo-Gómez (Department of Medicine, School of Medical Sciences, Universitat Jaume I, Vicente Sos Banyat s/n, 12071 Castellón de la Plana, Spain. e-mail: escastil@uji.es)

NUMBER OF FIGURES: 7 + 1 supplementary figure

KEYWORDS: 2-photon, spine dynamics, en passant boutons, axonal dynamics, pyramidal neuron, barrel cortex, recognition memory, TrkB receptor

ABSTRACT

BDNF and its receptor TrkB have important roles in neurodevelopment, neural plasticity, learning and memory. Alterations in TrkB expression have been described in different CNS disorders. Therefore, drugs interacting with TrkB, specially agonists, are promising therapeutic tools. Among them, the recently described 7,8-dihydroxyflavone (DHF), an orally bioactive compound, has been successfully tested in animal models of these diseases. Recent studies have shown the influence of this drug on the structure of pyramidal neurons, specifically on dendritic spine density. However, there is no information yet on how DHF may alter the structural dynamics of these neurons (i.e. real-time study of the addition/elimination of dendritic spines and axonal *boutons*). In order to gain knowledge on these effects of DHF, we have performed a real-time analysis of spine and axonal dynamics in pyramidal neurons of barrel cortex, using cranial windows and 2-photon microscopy during a chronic oral treatment with this drug. After confirming TrkB expression in these neurons, we found that DHF increased the gain **rates** of spines and axonal *boutons,* as well as improved object recognition memory. These results help to understand how the activation of the BDNF-TrkB system can improve basic behavioural tasks through changes in the structural dynamics of pyramidal neurons. Moreover, they highlight DHF as a promising therapeutic vector for certain brain disorders in which this system is altered.

INTRODUCTION

The receptor of the brain-derived neurotrophic factor (BDNF), the tropomyosin receptor kinase B (TrkB), is expressed in most of the pyramidal neurons of the neocortex (Miller and Pitts 2000). The interaction of this neurotrophin and its receptor is not only essential for neural growth and survival, but also for neural plasticity (Yoshii and Constantine-Paton 2010), in which, among other functions, it promotes synaptic potentiation through the establishment of LTP in the cerebral cortex (Kang et al. 1997; Escobar et al. 2003). However, its malfunction underlies the etiopathology of different neuropsychiatric disorders, including major depression (Castrén and Rantamäki 2010) or schizophrenia (Pandya et al. 2013). Therefore, it is important to develop strategies to activate TrkB that could be clinically implemented. In this regard, the 7,8-dihydroxyflavone (DHF), a potent and specific TrkB agonist, has recently emerged as a promising therapeutic treatment (Jang et al. 2010). This drug is especially interesting because it is orally bioactive and can easily cross the blood-brain barrier (Du and Hill 2015). In fact, recent research has already proven its effectiveness in animal models of Parkinson's disease (Jang et al. 2010), Alzheimer's disease (Zhang et al. 2014; Castello et al. 2014), major depression (Zhang et al. 2015; Zhang et al. 2016) or schizophrenia (Yang et al. 2014). Given the involvement of BDNF/TrkB in neuronal plasticity it is thought that DHF would increase it. However, the neurobiological bases of these positive effects on plasticity are still not fully understood.

Although neural plasticity can be studied from different points of view, changes in neuronal structure should represent the rearrangement of synapses and, therefore, in the neural circuitry (Caroni et al. 2012). Regarding this, different studies have shown that DHF reverts the structural alterations found in the pyramidal neurons of certain animal models of CNS disorders: It returns to control levels the decreased spine density in mouse models of Alzheimer's disease (Castello et al. 2014) and major depression (Zhang et al. 2015). Moreover, in healthy rats, DHF reverts the functional

decline produced by ageing, probably by increasing the spine density in the amygdala, hippocampus and prefrontal cortex (Zeng et al. 2012a). However, the study of structural plasticity goes beyond these analyses of dendritic spine density. With the emergence of **imaging techniques for examining** structural dynamics we have increased our knowledge on how neuronal networks are finely modulated by different treatments. In order to perform such experiments, it is necessary to chronically implant cranial windows in mice that express a fluorescent protein in their pyramidal neurons and to image these cells in real-time with a 2-photon microscope (Holtmaat et al. 2009). These studies give us information in real-time of the addition, elimination or stability of dendritic spines and axonal *boutons*, such as the *en passant boutons* (EPB), in the same structure throughout an entire experiment (Holtmaat and Svoboda 2009; Chen and Nedivi 2013). They also allow us to distinguish transient alterations from persistent ones. This represents valuable information for understanding long lasting changes in the network (Holtmaat et al. 2006; Holtmaat and Svoboda 2009; Chen and Nedivi 2013), since the spines that remain stable for at least 4 days are the ones that always bear a synapse (Knott et al. 2006). In addition, these analyses are **longitudinal** and consequently may allow us to establish the proper treatment course for further clinical research on the drug tested. Alterations in structural dynamics have been proposed to underlie adaptation to changing environments, as has been shown after sensory deprivation in both excitatory (Hofer et al. 2009; Holtmaat and Svoboda 2009; Cane et al. 2014) and inhibitory (Chen et al. 2011c; Chen et al. 2011b; Keck et al. 2011; Chen et al. 2012; van Versendaal et al. 2012) circuits.

We have developed an experiment to understand how BDNF/TrkB interaction regulates in real-time the neuronal structural plasticity of pyramidal neurons in the barrel cortex and affects behaviors **presumably** dependent on this cortical region. Thy1-YFP transgenic mice, in which a subset of layer V pyramidal neurons constitutively express EYFP (Feng et al. 2000; Porrero et al. 2010) were used in this

study. We have imaged in real-time the same dendrites and axons before and during a 14-day treatment with DHF and have tested anxiety-related behaviors and object recognition memory.

MATERIAL AND METHODS

Animals and 7,8-Dihydroxyflavone treatment

Twenty-six adult transgenic mice Thy1-YFP, line H (Jackson Laboratories; Bar Harbor, Maine, USA) were used for all the experiments **(Fig. 1a)**. In this strain, layer V cortical pyramidal neurons are densely labeled with EYFP (Feng et al. 2000) (**Fig. 1b**). Two of these mice were destined to the analysis of TrkB expression in Thy1-YFP expressing neurons (see below). Cranial windows were implanted in the remaining 24 mice to study in real-time the effects of the treatment with the TrkB agonist 7,8-Dihydroxyflavone (DHF, Abcam, Cambridge, UK) on the structural dynamics of Thy1-YFP expressing neurons (**Figs. 1a-1d**). The behavior of these 24 animals was also evaluated on the open field arena and the novel object recognition test (**Figs. 1e&f)**. However, only mice carrying cranial windows that remained clear during the whole experiment were taken into account in both the structural and behavioral analyses (6 in the control group and 9 in the DHF group). These mice were subjected to 3 consecutive 2-photon imaging sessions before starting the DHF or vehicle treatment and 3 sessions during the treatment (see below and **Fig. 1**). The oral treatment with DHF or with vehicle solution started right after the end of the 3rd imaging session. Eighty microliters of a DHF (100 mg/ml in DMSO; Abcam) or vehicle solution (DMSO; Sigma-Aldrich, San Luis, MO, USA) were added to 100 ml of drinking water containing 1% of sucrose (pH=7.4). These solutions were replaced every 3-4 days during the 14 days of duration of the treatment and bottle content was measured to monitor liquid intake. Animals were also weighted every 3-4 days. The average liquid intake was 2

ml/day/mouse and the average weight of mice was 32 g. Therefore, DHF dose was approximately 5mg/kg/day.

Animals were reared in groups of 3-4, in standard-size polycarbonate cages, in a temperature- and humidity-controlled environment and maintained on a 12 h light/dark cycle with food and water available *ad libitum*.

All animal experimentation was conducted in accordance with the Directive 2010/63/EU of the European Parliament and of the Council of 22 September 2010 on the protection of animals used for scientific purposes and was approved by the Committee on Bioethics of the Universitat de València. Every effort was made to minimize the number of animals used and their suffering.

TrkB immunohistochemistry

Thy1-YFP mice destined to the analysis of TrkB expression in YFP expressing pyramidal neurons were transcardially perfused with 4% paraformaldehyde solution and their brains were cut in 50 µm-thick coronal sections using a vibratome (Leica VT1000E, Leica, Wetzlar, Germany). Free-floating sections were first blocked with 10% normal donkey serum solution and then incubated overnight at room temperature with goat anti-TrkB receptor primary antibody (1:400; R&D systems, Minneapolis, MN, USA). The day after, sections were incubated with donkey anti-goat secondary antibody conjugated with AlexaFluor®647 (1:400, LifeTechnologies, Carlsbad, CA, USA) for 2 hours and then mounted on slides and covered with mounting media (Dako, Glostrup, Denmark). Images were acquired with a Leica TCS SPE confocal microscope using a 63X oil objective and 2X digital zoom magnification (**Fig. 2**).

Cranial window implantation

To allow long-term high-resolution imaging of *in vivo* neuronal morphology, a cranial window was unilaterally implanted over the primary somatosensory cortex (barrel field;

Bregma -1.5 mm, Lateral 3.5 mm) of 24 Thy1-YFP mice (2-month-old). Animals were first anesthetized with an intraperitoneal injection of a mixture of ketamine (50 mg/kg; Imalgene, Merial, Lyon, France) and medetomidine (1 mg/kg; Sedator, Dechra, Barcelona, Spain); carprofen (5 mg/kg; Rimadyl, Pfizer, New York, NY, USA) was also injected intraperitoneally to avoid inflammation, and a subcutaneous injection of butorphanol (5 mg/kg; Torbugesic, Pfizer) was administered to avoid any suffering during and after the surgery. Animals were placed afterwards in a stereotaxic device. After cutting a flap of skin (approx. 1 cm^2), the periosteum was gently removed from the skull using fine tweezers and the *temporalis* muscle was separated with a blunt spatula. A thin layer of cyanoacrylate was applied to the *temporalis* muscle, wound margins and skull, with the exception of the region of interest in the skull. Once it dried, a thin layer of dental acrylic was applied on top of the glue. A circular groove around the area of interest was pierced using a biopsy punch with a diameter of 3 mm (Aesthetic Group, Puiseux-le-Hauberger, France) leaving an island of skull in the center that was removed afterwards using the tip of sharp forceps. **This technique was chosen because it produces less harm in the underlying nervous tissue than the classical drill technique used in open-skull surgeries. However, further assays (study of the presence of reactive glia) were performed in order to confirm the absence of damage.** To clean the area, drops of cortex buffer (Holtmaat et al. 2009) were applied regularly after the island of skull was removed. Finally, the unblemished dura was covered with a circular coverglass (3 mm diameter, 1 mm thick; Harvard Apparatus, Holliston, MA, USA) and the borders were sealed with cyanoacrylate and dental acrylic. Finally, animals were intraperitoneally injected with atipamezole (0.5 mg/kg; Antisedan, Esteve, Barcelona, Spain) to revert the anesthesia and returned to individual cages for recovery. The day after surgery, mice were returned to their home cages (social rearing) and left undisturbed for 2 weeks to allow complete recovery before imaging.

Assessment of the presence of reactive astroglia and microglia in the parenchyma underlying cranial windows

Because the employment of biopsy punches to perform the cranial windows is a novel technique, two animals were processed to search for gliosis under the cranial window. The ipsilateral hemispheres to the cranial window of these mice were cut in 100-µm-thick coronal sections using a vibratome (Leica VT1000E, Leica), and the slices where processed to detect astroglia and microglia and the presence of reactive gliosis. Therefore, an immunohistochemistry assay was performed using markers for these types of cells. The same immunohistochemistry protocol described before was applied using as primary antibody the mouse IgG anti-S100 (1:1000, Sigma-Aldrich), a marker of astrocytes, and the biotin-conjugated lectin from *Lycopersicon esculentum* (1:50, Sigma-Aldrich), a marker of microglial cells. These markers were subsequently detected with goat anti-mouse IgG AlexaFluor®405 (LifeTechnologies) and Streptavidin AlexaFluor®647 (LifeTechnologies) respectively. Slices were mounted on slides and covered with mounting media (Dako). Images were acquired using an Olympus FV1000 confocal microscope (Olympus, Tokyo, Japan) using a 60X oil objective and 1.3X digital zoom magnification.

In vivo 2-photon imaging

In vivo 2-photon imaging was achieved using an Olympus FV1000MPE microscope and its acquisition software (Olympus fluoview FV1000 v4.0.1.10, Olympus). The light source for 2-photon excitation was a commercial Ti:Sapphire laser (Mai-Tai HP DeepSee, Spectra Physics, Santa Clara, CA, USA). The excitation wavelength was set to 930 nm, with the excitation signal passing through an XLPLN25XWMP 25×/1.05 NA water-immersion objective (Olympus) and collected after a barrier filter by a

photomultiplier tube. The same cells could be identified and re-imaged for up to 20 days using local fiduciary landmarks of the brain's surface vasculature.

Image acquisition and analysis

Adult mice (3-month-old) previously implanted with cranial windows were anesthetized with a mixture of ketamine (50 mg/kg; Imalgene, Merial) and medetomidine (1 mg/kg; Sedator, Dechra). Anesthesia was monitored by breathing rate and foot-pinch reflex. A total number of 15 mice presented a cranial window clear enough to complete all the imaging sessions. The head was positioned in a custom-made stereotaxic restraint. In the first imaging session, a panoramic z-stack was obtained in order to identify all the landmarks and regions of interest (512x512, z step-size 3 μm). Afterwards, 4 regions of interest were imaged per animal, each of them containing several dendrites and axons. These images were obtained with a digital zoom of 8X and comprised only layer I of the neocortex (512x512, z step-size 1 μm). Raw scanner data were processed in ImageJ (National Institutes of Health, Bethesda, MD, USA) and the 6 four-dimensional (x, y, z, t) stacks of each animal were analyzed blind to the experimenter using this software.

The real-time analysis included 6 dendrites and 6 axons of pyramidal cells per mouse, so that each animal would present uniform data regarding their dynamics, resulting in a total of 344 axonal *boutons* and 1699 dendritic spines in 90 axons and 90 dendrites (approximately 23 axonal *boutons* and 113 spines per animal). The regions of interest were arbitrarily named with a two-letter code to avoid any bias from the experimenter. Dendritic and axonal branches were distinguished by their morphology. Axons were typified as thin tubular processes, often scattered with varicosities (EBP) whose fluorescence were at least 2 times higher than that of the axonal backbone. Dendrites were distinguished by thicker diameters (generally >2 μm), smooth, gradually tapering processes, and characteristic branching patterns. Their dendritic spines were scored

manually as membranous protrusions obeying to two criteria: (1) they should be unilateral and (2) they should be longer than 0.8 µm, measured from the emergence of the spine to its tip.

In order to study the structural dynamics, several parameters were analyzed. Gain, loss and stability **rates** were respectively the new, lost and stable spines/EPB in a given time point related to the previous number of spines/EPB (**Fig. 1d**). The turnover **rate** was the sum of the gain and loss **rates** divided by 2, which provided us with a more accurate idea about the dynamism. The stable **rates** were also studied because of their importance for the network, since structures lasting longer than 4 days have been shown to always bear at least one synapse (Knott et al. 2006; De Paola et al. 2006; Grillo et al. 2013). The stable gain **rate** represented the number of structures (spines and EPBs) added in a time point and lasting for at least 4 days (2 consecutive imaging sessions), related to their previous number. Likewise, the stable loss **rate** of spines/EPB represented the structures that have lasted longer than 4 days (2 consecutive imaging sessions) and were then lost, related to their previous number (**Fig. 1d**). The turnover **rate** of stable spines/EPB was the sum of the gain and loss **rates of stable spines/EPB** divided by 2 and, again, provides us with a more accurate idea about the dynamism. After all the dynamic **rates** were calculated, they were divided by their first data point in order to normalize them and were multiplied by 100 to be expressed in percentages –related to the previous number- of dendritic spines or EPB **that have been gained, lost, remained stable or experience some turnover. Therefore, the first data point of each data set is set to 100%: -8d/-4d when addressing the "normal" dynamic parameters, -8d→-4d/0d when addressing the loss rate of stable spines/EPB, -8d/-4d→0d in the case of spines/EPB that are gained and remain stable, and -8d→-4d/-4d→0d] when studying the turnover rate of stable spines/EPB.**

Spine volume analysis

It has already been shown that the fluorescence intensity of a spine head is positively correlated to its volume (Holtmaat et al. 2005). In fact, increases in spine volume are related to potentiation via LTP, whereas the dendritic shaft remains unaffected (Matsuzaki et al. 2004). Therefore, we analyzed whether the dendritic spines that were stable throughout the experiment would alter their volume during the DHF treatment. 6 stable spines were studied per animal (a total of 90 spines). This procedure diminished intra-group variability. Additionally, the images should not contain saturated pixels in order to allow for the detection of variations in fluorescence intensity (pixel value). Because the intensity of the overall image could be altered due to changes in the conditions of 2-photon imaging or the cranial window, the intensity of the dendritic shaft, which volume remains unaffected, was also taken into account (Svoboda et al. 1996; Trachtenberg et al. 2002). **We then chose the focal plane with the highest integrated fluorescence across the spine** and calculated the ratio between its mean pixel value and the mean pixel value of a similar portion of the adjacent dendritic shaft. **In addition, the standard deviation of the point spread function was calculated for each spine using ImageJ (National Institutes of Health), and these data were statistically compared to ascertain our measures were not influenced by uncontrolled factors.**

Behavioral tests

Twenty-four hours before starting the *Novel Object Recognition* (NOR) test, all animals were exposed for 10 minutes to the empty apparatus (*Open Field chamber,* OF*, 40x40cm)* (**Figs. 1&3**). This habituation procedure was also used to evaluate the locomotor activity and the anxiety levels of the animals (ANY-maze video tracking system v4.98; Stoelting Europe, Dublin, Ireland), in order to remove from the experiment those mice showing abnormal behaviors. The video tracking system provided automated measures of the total distance travelled and mean speed, to study locomotor activity, and number of entries and time spent in the periphery of the arena,

for the measurement of anxiety and thigmotaxis (a valid index of anxiety in mice; Simon et al. 1994). The periphery zone of the arena was defined as the area located between 0 and 6 cm from the walls of the apparatus. All animals were subjected to the OF (day -1 and day 12) and NOR (day 0 and day 13) tests before and after the treatment with DHF or vehicle solution (**Fig. 1**).

Every NOR test was divided in 2 sessions or phases: "*familiarization*" and "*test*" (**Figs. 1&4**). During the *familiarization phase*, two copies of an object (familiar object) were placed in 2 opposite corners of the OF arena (5 cm away from the walls) and the animal was allowed to explore the arena for 4 minutes. During the *test phase* (30 seconds after the familiarization phase), a duplicate of the familiar object and a novel object were placed in opposite corners of the arena and mice were allowed again to explore the open field arena for 4 minutes. Between sessions, the apparatus and all objects were cleaned with 70% ethanol solution to eliminate odor cues. In this experiment, all mice participated in 2 familiarization phases and 2 test phases, one for every level of perceptual difficulty ("Easy" and "Difficult"; **Fig. 1**) (Burke et al. 2011; Burke et al. 2012). In the "*Easy task*" the novel and familiar object did not share any common features, this is, they were different in shape, texture and size (**Figs. 4a&b)**. For the *"Difficult task"*, the objects were identical in shape and color and only 1 of the sides of the objects had a different texture (**Figs. 2a&b**). This difficult task was designed to analyze object recognition dependent on the barrel cortex. Object exploration was scored whenever the mouse sniffed the object or touched the object while looking at it (when the distance between the nose and the object was less than 2 cm). Climbing onto the object or chewing the object did not quantify as exploration (Leger et al. 2013). The time spent exploring each object was recorded during the habituation and test phases in both levels of perceptual difficulty (easy and difficult). For every animal, the data of the test phase was normalized with the data of the habituation phase to calculate afterwards the discrimination ratio (DR) in the easy and

difficult task: time spent exploring the novel object divided by the time spent exploring both the novel and familiar objects (Bevins and Besheer 2006).

Statistics

All the dynamic parameters were normalized to time -8d (first imaging session) prior to the statistical analysis, **thus converting all the dynamic data in percentages related to the previous data point and being the first one 100%.** For all the **longitudinal** studies, a repeated-measures ANOVA was performed with treatment (DHF vs control) as between-subjects factor and time (imaging sessions) as within-subjects factor, followed by *post hoc* tests (Fisher's least significant difference) for pairwise comparisons. The unit of observation was always the animal, and each data point in the linear analysis of structural dynamics was the mean of the dynamics of 6 different structures (dendrites, axons or dendritic spines), which diminished the intra-group variability. Only mice that finished all the imaging sessions were taken into account and the same animals with completed structural analysis were used to analyze the behavioral tests (6 control and 9 DHF).

Behavioral data were analyzed using repeated measures ANOVA followed, when appropriate, by post-hoc test. When analyzing the OF data, treatment (DHF vs control) and time (**before vs after DHF-treatment**) were considered as a between-subjects and within-subjects factors respectively. In the NOR test, an extra within-subjects factor (Difficulty: easy vs difficult task) was added to the analysis.

All the statistical analyses were performed using the statistical package SPSS v22.0 (IBM) and graphs were created using GraphPad Prism 6. Data in the figures were expressed as mean ± SEM and $p<0.05$ were indicated.

RESULTS

Pyramidal neurons of the barrel cortex express TrkB in their somata, dendritic spines and axonal boutons

We performed immunohistochemistry to demonstrate that TrkB was expressed by pyramidal neurons of the barrel cortex in Thy1-YFP mice (**Fig. 2**). We found that, indeed, TrkB expression puncta were found inside and in close apposition to axonal en *passant boutons* (**Fig. 2b**), the cell somata (**Fig. 2c1**), as well as in spine heads (**Fig. 2c2**).

Cranial windows performed with the biopsy punch do not elicit gliosis

In order to detect whether our cranial windows were producing damage in the underlying neocortical parenchyma, we studied the distribution and morphology of astrocytes and microglia with immunohistochemistry. We observed that both cells displayed similar density and morphology when comparing layer I and V from regions below the cranial window with regions of the neocortex located outside the influence of the surgery (Supp. fig 1). No reactive astrocytes or microglia were observed in any of the regions studied.

DHF treatment does not affect locomotion or anxiety-related behavior

We analyzed the distance travelled, mean speed and immobility time during the OF test, before (day-1) and after (day 12) **vehicle or DHF treatments**, as an index of locomotor activity (**Figs. 3a&b**). Although decreased locomotion was found to occur after the treatment (distance travelled, mean speed and immobility time; **Fig. 3b**), no statistically significant differences were found between DHF and vehicle-treated mice (distance travelled at day -1 or at day 12, **Figs. 3a&b;** mean speed at day -1 or at day 12; **Fig. 3b**; and immobility time at day -1 or day 12, **Fig. 3b**).

A similar situation occurred when we analyzed anxiety-related behavior (**Fig. 3c)**, with an apparent decrease of anxiety after treatment (border distance, border time and line crossings), but no statistically significant differences among DHF and control groups were found.

DHF treatment improves object recognition

When we analyzed the discrimination ratio (time spent exploring the novel object/ time spent exploring both objects), repeated measures ANOVA showed a statistically significant effect of time (before vs after treatment: p=0.013, **Figs. 4a&b)** and Time*Treatment interaction (0.002) only for the difficult condition. Therefore, multiple pairwise comparisons could only be performed for the difficult condition. We found that the DHF group of mice did not show statistically significant differences with the control group before treatment (day 0) but showed an increased object discrimination ratio 13 days after treatment in the difficult task. **Therefore, only DHF-treated mice showed increased object discrimination ratio in the difficult task** (**Fig 4b**).

Chronic DHF treatment alters the dynamics of axonal* boutons *in pyramidal neurons of the barrel cortex

Different dynamic and stability parameters were analyzed and found altered during the DHF treatment (**Fig. 5**). The gain **rate** of EPB was altered during the experiment in both experimental and control conditions, although in a different direction (**Fig. 5b**). In control conditions the gain **rate** diminished gradually throughout the experiment **(i.e. the rate by which new spines were formed was progressively decreasing)**, whereas in DHF-treated mice it was firstly increased and finally decreased to baseline levels. The difference between groups reached its peak in the middle of the DHF treatment (4d/8d)**.** Neither the loss **rate** nor the turnover **rate** were altered during the experiment. However, in the DHF group the stability **rate** of their EPB decreased

gradually through the treatment **(i.e. the rate of EPB that remained stable from one time point to the next one was reduced progressively during the experiment)**.

We next asked whether the stable EPB (**those that last longer than 4 days**) presented altered dynamics due to the DHF treatment, and found several interesting variations (**Fig. 5c**). First, the gain **rate** of stable EPB increased rapidly only in the beginning of the DHF treatment, **which means that the rate by which EPB were formed and became stable (lasting longer than 4 days) was increased right after the beginning of DHF treatment**. By contrast this rate remained unchanged in control conditions. Second, the **loss rate of stable EPB (those that last at least 4 days, but are lost afterwards)** increased gradually throughout the experiment in both conditions (**i.e. the rate of disappearance of stable EPB increased progressively through the DHF and control conditions**). However, in the DHF-treated mice this increase was more consistent, and there was a trend towards an increase in the DHF group in the middle of the treatment (0d→4d/8d) when compared with the control group. Finally, the turnover **rate** of stable EPB was increased in the beginning of the experiment in control conditions, **which means that right after the start of the real-time imaging sessions the rate by which stable EPB were gained and lost rose;** whilst in the DHF group this **increase** was significant from its baseline to the end of the DHF treatment.

Chronic DHF treatment alters the dynamics of dendritic spines in pyramidal neurons of the barrel cortex

In order to further understand the dynamics of pyramidal neurons under the influence of DHF, we analyzed the dendritic spine dynamics throughout the treatment (**Fig. 6b**). We found that the gain **rate** rapidly increased in the beginning of the experiment but later decreased to baseline and control levels **(i.e. the rate by which spines were appearing increased right after the beginning of the experiment and later returned to control levels)**. There was also a trend towards an increase in the DHF

group in the middle of the treatment (4d/8d) when compared with the control group. The turnover **rate** was first increased in DHF animals, to return finally to control and baseline levels **(i.e. the rate of spine addition and elimination increased until 4 days after the beginning of the treatment and decreased thereafter)**. **Furthermore, the loss rate increased in the beginning of the treatment only in control conditions**, whereas the stability **rate** was reduced in both Control and DHF groups, although more prominently so in the former.

Chronic DHF treatment protects stable pyramidal spines from dynamic changes

We next asked whether the stable spines (**those that last longer than 4d**) had their dynamics altered under the DHF treatment (**Fig. 6c**). The gain **rate** remained unaltered, **meaning that the rate of appearance of dendritic spines did not change**. However, the loss **rate** and the turnover **rate** of stable spines varied in control conditions. The loss **rate** of stable spines increased throughout the experiment **(i.e. the rate by which stable spines were disappearing progressively increased).** These increases were also significant when comparing DHF and Control groups (0d→4d/8d and 4d→8d/12d), and there was also a trend towards an increase at the beginning of the treatment (-4d→0d/4d). Similarly, the turnover rate of stable spines was altered only in control conditions, first increasing and later returning to baseline levels, which means that **the rate of addition and elimination of stable spines increased until the beginning of the vehicle treatment and decreased thereafter.** There were also trends towards an increase when comparing both groups in the middle of the treatment (-4d→0d/0d→4d and 0d→4d/4d→8d).

The volume of pyramidal spines remains unaltered throughout the DHF treatment

In order to better understand **the increases in the loss rate of stable spines, and alterations in the turnover rate, only in control conditions;** we estimated the

volume of the spines that were present throughout the entire experiment (**Fig. 7**). **These analyses were performed after confirming that the standard deviation of their point spread function did not statistically change, thus making sure the image analyzed was a reliable representation of the real object.** Surprisingly, we found that the stable spines of the control group increased their volume whereas in DHF-treated mice this parameter remained stable. These increases were significant within the control group and when comparing both groups (4d).

DISCUSSION

In the current study, we show, in real-time, how the structure of neocortical pyramidal neurons is altered during a chronic treatment with DHF, a TrkB agonist that has an important clinical potential **(Fig. 8).** Furthermore, we show that this treatment also enhances the recognition of complex objects.

Our findings are in agreement with previous reports that showed the expression of TrkB in layer V in pyramidal neurons of the rat somatosensory cortex (Miller and Pitts 2000). Moreover, we expand this knowledge by describing the presence of the receptor in the somata, dendritic spines and axonal *boutons* of these neurons in mice. We next asked whether a chronic activation of TrkB would alter the dynamics of these neuronal structures (gain, loss, stability **rates** of dendritic spines and axonal *boutons* in a longitudinal, chronic real-time study). We also wondered whether it would impact behaviors **presumably** dependent on this brain region. The gain **rate** of dendritic spines was increased 4 days after the beginning of the treatment, persisted after 8 days and returned to baseline levels 12 days afterwards. Our findings are consistent with previous electrophysiological and structural findings, since LTP can be induced by TrkB activation (Minichiello et al. 2002; Minichiello 2009) and this form of synaptic plasticity promotes the apparition of dendritic spines in pyramidal neurons (Engert and Bonhoeffer 1999). In addition, pyramidal spine density increases in the rat hippocampus after BDNF administration (Tyler and Pozzo-Miller 2003), and also after a chronic treatment with DHF (Zeng et al. 2012b). However, all these previous findings were performed in post-mortem tissue and thus alterations in spine dynamics cannot be inferred.

We have also studied the dynamics of stable spines, which are those present at least for 4 days (two consecutive imaging sessions). These spines are particularly important because they have been shown to always bear a synapse (Knott et al. 2006) and, therefore, are the ones modifying the network. The loss **rate** of stable spines

(spines lasting longer than 4 days, which are then lost) was incremented during our experiment only in the control group, whereas in the DHF treated animals there were no changes. Surprisingly, only in **the** control group, we have also found that the spines that remained stable during the whole experiment increased their volume. This enlargement in the remaining spines may be the consequence of the synaptic loss caused by the elimination of stable spines. Since increases in spine volume have been previously correlated to spine potentiation (Matsuzaki et al. 2004), we suggest that these remaining stable spines increase their volumes in order to compensate and maintain synaptically the circuit.

We have also shown that the stability **rate** of dendritic spines was gradually reduced throughout the experiment, **and this reduction was more pronounced** in control animals. **Likewise, the loss rate of dendritic spines was increased in the beginning of the experiment only in control mice.** These two facts appear to be a consequence of real-time imaging: similar reductions in the stability rate have already been shown in the same mice strain that we used (Grutzendler et al. 2002). Consequently, it is likely that DHF might protect against the intrinsic damage that real-time imaging produces, which is in agreement with the known neuroprotective properties of this drug against glutamate excitotoxicity (Chen et al. 2011a), neonatal hypoxia, ischemia (Uluc et al. 2013), degeneration of dopaminergic neurons in animal models of Parkinson's disease (Luo et al. 2016) or staurosporine-induced apoptosis (Jang et al. 2010).

The dynamics of axonal *boutons* were also analyzed before and during DHF treatment, showing increases in their gain **rate** 8 days after its onset. The dynamics of stable EPB (**EPB that last longer than 4 days**) were also analyzed and we found that their gain **rate** increases. Both results agree with the increases in axonal arborization, and consequently in the presynaptic surface, that BDNF infusion produces in other

species (Cohen-Cory and Fraser 1995; Lom and Cohen-Cory 1999; Bing et al. 2005; Granseth et al. 2013).

We have also wondered whether a chronic treatment with DHF might improve sensory perception, **which is mostly** dependent on the barrel cortex, the region of our structural analysis. In order to study this, we have performed a modified NOR test with easy and difficult novel objects that varied in their texture, so that they may be mostly recognizable by their whiskers (Guić-Robles et al. 1989; Arabzadeh et al. 2005; Brecht 2007; von Heimendahl et al. 2007). We have found that, indeed, animals treated with this drug displayed a higher discrimination ratio **(time spent exploring the novel object/ time spent exploring both objects)**. These results agree with multiple studies correlating BDNF or TrkB manipulation with object recognition memory: BDNF expression has been positively linked to object recognition memory (Hopkins and Bucci 2010), whereas a lesser activation of TrkB with anti-BDNF produces opposite results (Callaghan and Kelly 2013). In addition, DHF has already been shown to improve memory consolidation in both rats and mice also in a NOR test (Bollen et al. 2013). Our results go further and show that DHF also enhances object recognition behavior and sensory discrimination. **Although our results suggest a connection between the effects of DHF treatment on neuronal structure and those on object recognition, it is possible that these two effects were concurrent but not connected.**

In conclusion, we provide real-time *in vivo* evidence of how the chronic activation of TrkB has beneficial behavioral effects in healthy animals and alters the structural plasticity and dynamics of neocortical pyramidal neurons. Our results also highlight the timeline of these structural changes, so that further research can pinpoint the optimal duration of the treatment. This is not unimportant since the malfunction of the BDNF-TrkB system has been suggested to underlie several neuropsychiatric disorders, including Alzheimer's disease or schizophrenia (Angelucci et al. 2005; Zuccato and

Cattaneo 2009), and currently its manipulation is being tested to provide new therapeutic vectors for these diseases (Nagahara and Tuszynski 2011; Lu et al. 2013).

FIGURE LEGENDS

Fig. 1 Experimental design. (a) Timeline of the experimental procedure **(b)** To allow long-term and high-resolution imaging of *in vivo* neuronal morphology of pyramidal neurons, a cranial window was unilaterally implanted over the primary somatosensory cortex (S1; Bregma -1.5 mm, Lateral 3.5 mm) of Thy1-YFP mice (2-month-old). **(c)** Twenty days after surgery, 2-photon imaging sessions started. **(d)** The same dendrites and axons of every animal were imaged every 4 days to study spine and *en passant bouton* (EPB) dynamics. Every animal was recorded 3 sessions before and 3 sessions after DHF or vehicle treatment. Arrowheads point to dendritic spines or EPB with a color legend to clarify the effect on the dynamic parameters. White arrowheads point to spines/EPB that are present from the beginning of the experiment. Yellow arrowheads point to spines/EPB that are gained in that imaging session. Blue arrowheads point to those spines/EPB gained in the previous imaging session that have become stable. Red arrowheads point to EPB that were present in the previous imaging session but have disappeared in the current one. **(e)** To test locomotion and anxiety related behavior, all animals were evaluated in the OF test, 24 hours before starting the treatment and on the 12th day of treatment. **(f)** A modified version of the novel object recognition test was used to evaluate recognition memory in mice before (day 0) and after **DHF-treatment** (day 13). Novel objects are indicated in the scheme with an asterisk (see material and methods' section for further details)

Fig. 2 TrkB receptor expression in Thy1-YFP expressing neurons. (a) Confocal panoramic view of a Thy1-YFP brain slice (Bregma -1.22 mm) immunostained for TrkB receptor (red). Our region of interest, the primary somatosensory cortex (S1) is delimited by the 2 dotted lines. Scale bar: 800 µm. **(b)** Magnified view (12x) of the squared section in A, showing TrkB expressing puncta (arrowheads in B1') co-localizing or in close apposition to YFP expressing axonal *boutons* (green). **(c)** 4.5x magnification of the squared area in A, showing layer V YFP-expressing pyramidal

neurons. TrkB receptors were found surrounding and in close apposition to the somata of these neurons (arrowheads in c1') as well as to the spine head (c2')

Fig. 3 Open field test (OF). (a) Representative track-plot reports recorded during the 10 min test sessions (ANY-maze). The central square was denominated "central zone" and the periphery, "border zone". Observe the decrease in the distance traveled (purple line) by both groups (DHF and control) after the treatment **(distance travel: $p=1.2*10^{-5}$, mean speed: $p=1.3*10^{-5}$, immobility time: $p= 1.0*10^{-6}$)**. Locomotor activity **(b)** and anxiety-related behavior **(c)** were decreased in both groups after the treatment **(border distance: p=0.051, border time: p=0.095, line crossings: p=0.008)**, but no significant differences were found between them. (***) p<0.001; (#) 0.1>p>0.05

Fig. 4 Novel object recognition test (NOR). (a) Schematic drawings of the 2 types of NOR tests performed in our experiment and their phases (familiarization: 2 identical objects; test: 1 familiar and 1 novel object). **(b)** Photographs of the pairs of objects that were randomly used during the NOR test. The asterisk marks the novel object. (**c)** Bar graphs representing the discrimination ratio [time spent exploring the novel object/ time spent exploring both objects] for the easy and difficult tasks of the NOR test before (day 0) and after DHF treatment (day 13). Only DHF treated mice showed increased object discrimination ratio in the difficult task **(p=0.017)**. Black Horizontal lines in graphs represent statistically significant effects of time (black), treatment (gray), or Time*treatment interaction (black, dashed) in a repeated-measures ANOVA (*p<0.05, **p<0.01, # 0.1<p<0.05)

Fig. 5 Structural dynamics of EPB prior and during the chronic DHF treatment. (a) Real-time 2-photon images of a representative axon from a DHF-treated mouse. Arrows point to EPB with a color legend to clarify the effect on the dynamic parameters. White arrows point to EPB that are present from the beginning of the experiment. Yellow arrows point to EPB that are gained in that imaging session. Blue arrows point to those EPB gained in the previous imaging session that have become stable. Red

arrows point to EPB that were present in the previous imaging session but have disappeared in the current one. Scale bar: 5 μm **(b)** Graphs representing the different dynamic parameters. **Gain rate: Longitudinal effects in the control group -8d/-4d vs 4d/8d: p=0.009; -4d/0d vs 4d/8d: p=0.09; and longitudinal effects on DHF group -8d/-4d vs 4d/8d: p=0.033; 0d/4d vs 4d/8d: p=0.047; 4d/8d to 8d/12d: p=0.019. Control vs DHF effects at 4d/8d: p=0.005. Stability rate: Longitudinal effects in the DHF group -4d/0d vs 8d/12d: p=0.018; 0d/4d vs 8d/12d: p=0.028.** **(c)** Graphs representing the different dynamic parameters studied only on stable EPB (those lasting longer than 4 days). **Gain rate of stable EPB: Longitudinal effects in the DHF group -8d/-4d→0d vs -4d/0d→4d: p=0.037. Loss rate of stable EPB: Longitudinal effects in the control group -8d→-4d/0d vs 4d→8d/12d: p=0.038; and longitudinal effects in the DHF group -8d→-4d/0d vs 0d→4d/8d: p=0.016, -8d→-4d/0d vs 4d→8d/12d: p=0.015, -4d→0d/4d vs 4d→8d/12d: p=0.015. Turnover rate of stable EPB: Longitudinal effects in the control group -8d→-4d/-4d→0d vs -4d→0d/0d→4d p=0.018; and in the DHF group -8d→-4d/-4d→0d vs 4d→8d/8d→12d: p=0.021.** (*) p<0.05; (**) p<0.01

Fig. 6 Structural dynamics of dendritic spines prior and during the chronic DHF treatment. (a) Real-time 2-photon images of a representative dendrite from a DHF-treated mouse. Arrows point to dendritic spines with a color legend to clarify the effect on the dynamic parameters. White arrows point to spines that are present from the beginning of the experiment. Yellow arrows point to spines that are gained in that imaging session. Blue arrows point to those spines gained in the previous imaging session that have become stable. Red arrows point to spines that were present in the previous imaging session but have disappeared in the current one. Scale bar: 10 μm. **(b)** Graphs representing the different dynamic parameters**. Gain rate: longitudinal effects in the DHF group -8d/-4d vs 0d-4d: p=0.032; -8d/-4d vs 4d/8d: p=0.037; -4d/0d vs 8d/12d: p=0.018; 0d/4d vs 8d/12d: p=0.018 and 4d/8d vs 8d/12d: p=0.016.**

Turnover rate: Longitudinal effects in the DHF group -8d/-4d vs -4d/0d: p=0.050; -8d/-4d vs 0d/4d: p=0.027; –4d/0d vs 8d/12d; p=0.036; 0d/4d vs 8d/12d: p=0.027. Stability rate: Longitudinal effects in the control group -8d/-4d vs 0d/4d: p=0.009; -8d/-4d vs 4d/8d: p=0.007; -4d/0d vs 0d/4d: p=0.005; -4d/0d vs 4d/8d: p=0.042; and in the DHF group 8d/-4d vs 0d/4d: p=0.014. **(c)** Graphs representing the different dynamic parameters performed only on stable spines (those that last longer than 4 days). **Loss rate of stable spines: Longitudinal effects in the control group -8d→-4d/0d vs -4d→0d/4d: p=0.010; -8d→-4d/0d vs 0d→4d/8d: p=0.004; -8d→-4d/0d vs 4d→8d/12d: p=0.006; and between control and DHF groups 0d→4d/8d: p=0.022 and 4d→8d/12d: p=0.010. Turnover rate of stable spines: Longitudinal effects in the control group -8d→-4d/-4d→0d vs -4d→0d/0d-4d: p=0.013; -8d→-4d/-4d→0d vs 0d→4d/4d→8d: p=0.019; -4d→0d/0d→4d vs 4d→8d/8d→12d: p=0.012; and 0d→4d/4d→8d vs 4d→8d/8d→12d: p=0.016.** (*) p<0.05; (**) p<0.01

Fig. 7 Real-time analysis of the dendritic spine volume prior and during the DHF treatment. (a) & (b) Low magnification images of representative dendrites in Control **(a)** and DHF-treated **(b)** animals. Scale bar: 6 µm. **(a') & (b')** High magnification images from the squared spines from Control **(a')** and DHF-treated **(b')** animals. Scale bar: 3 µm. **(c)** Graph representing the variation (%) in dendritic spine volume. **Longitudinal effects in the control group (-8d) vs 0d p=0.007, (-8d) vs 4d p=0.008, (-4d) vs 0d p=0.023, (-4d) vs 4d p=0.037 and between control and DHF groups at 4d p=0.014.** (*) p<0.05; (**) p<0.01

Fig. 8 Schematic drawing of the results on structural dynamics. Both panels show a dendrite (upper panel) or an axon (lower panel) before, in the middle of, and by the end of the DHF or Vehicle treatments. The addition (+), elimination (-) or stability (=) of dendritic spines (upper panel) or axonal *boutons* (lower panel) is represented in order to simplify the results on structural dynamics.

Supplementary figure 1 Absence of gliosis in the cortical region exposed to the cranial window. (a) Confocal panoramic view of a coronal slice from a THY1-YFP mouse chronically implanted with a cranial window. The surgery was performed with a biopsy punch. The edges of the cranial window have been indicated postmortem with small cuts. A subset of pyramidal neurons constitutively express EYFP (green), the microglia is labeled with tomato lectin (blue) and the cytoplasm of astrocytes is labeled with the antibody against S100 (red). Scale bar: 800 µm. **(a1) & (a2)** are higher magnification insets inside the window of layer 1 **(a1)** and layer 5 **(a2)**. **(a3) & (a4)** are similar insets taken outside the window also in layer 1 **(a3)** and layer 5 **(a4)**. Scale bar: 77 µm.

ACKNOWLEDGEMENTS

This work was supported by Generalitat Valenciana to JN (Prometeo Excellence Program PROMETEO2013/069) and CB-F (ACIF/2016/376), the Fundación Alicia Koplowitz to JN; and by the Spanish Ministry of Economy and Competitiveness to JN (SAF2015-68436-R), EC-G (IJCI-2015-24124) and MP-R (FPU12/03200).

COMPLIANCE WITH ETHICAL STANDARDS

Conflict of Interest: The authors declare that they have no conflict of interest.

All procedures performed in studies involving animals were approved by the Committee on Bioethics of the Universitat de València.

REFERENCES

Angelucci F, Brenè S, Mathé a a (2005) BDNF in schizophrenia, depression and corresponding animal models. Mol Psychiatry 10:345–52. doi: 10.1038/sj.mp.4001637

Arabzadeh E, Zorzin E, Diamond ME (2005) Neuronal encoding of texture in the whisker sensory pathway. PLoS Biol 3:e17. doi: 10.1371/journal.pbio.0030017

Bevins R a, Besheer J (2006) Object recognition in rats and mice: a one-trial non-matching-to-sample learning task to study "recognition memory". Nat Protoc 1:1306–1311. doi: 10.1038/nprot.2006.205

Bing H, Nikolakopoulou AM, Cohen-Cory S (2005) BDNF stabilizes synapses and maintains the structural complexity of optic axons in vivo. Development 132:4285–4298. doi: 10.1242/dev.02017

Bollen E, Vanmierlo T, Akkerman S, et al (2013) 7,8-Dihydroxyflavone improves memory consolidation processes in rats and mice. Behav Brain Res 257:8–12. doi: 10.1016/j.bbr.2013.09.029

Brecht M (2007) Barrel cortex and whisker-mediated behaviors. Curr Opin Neurobiol 17:408–416. doi: 10.1016/j.conb.2007.07.008

Burke SN, Ryan L, Barnes CA (2012) Characterizing cognitive aging of recognition memory and related processes in animal models and in humans. Front Aging Neurosci 4:1–13. doi: 10.3389/fnagi.2012.00015

Burke SN, Wallace JL, Hartzell AL, et al (2011) Age-Associated Deficits in Pattern Separation Functions of the Perirhinal Cortex : A Cross-Species Consensus. Behav Neurosci 125:836–847. doi: 10.1037/a0O25238

Callaghan CK, Kelly ÁM (2013) Neurotrophins play differential roles in short and long-

term recognition memory. Neurobiol Learn Mem 104:39–48. doi: 10.1016/j.nlm.2013.04.011

Cane M, Maco B, Knott G, Holtmaat A (2014) The relationship between PSD-95 clustering and spine stability in vivo. J Neurosci 34:2075–86. doi: 10.1523/JNEUROSCI.3353-13.2014

Caroni P, Donato F, Muller D (2012) Structural plasticity upon learning: regulation and functions. Nat Rev Neurosci 13:478–490. doi: 10.1038/nrn3258

Castello NA, Nguyen MH, Tran JD, et al (2014) 7,8-Dihydroxyflavone, a Small Molecule TrkB Agonist, Improves Spatial Memory and Increases Thin Spine Density in a Mouse Model of Alzheimer Disease-Like Neuronal Loss. PLoS One 9:e91453. doi: 10.1371/journal.pone.0091453

Castrén E, Rantamäki T (2010) The role of BDNF and its receptors in depression and antidepressant drug action: Reactivation of developmental plasticity. Dev Neurobiol 70:289–297. doi: 10.1002/dneu.20758

Chen J, Chua KW, Chua CC, et al (2011a) Antioxidant activity of 7,8-dihydroxyflavone provides neuroprotection against glutamate-induced toxicity. Neurosci Lett 499:181–185. doi: 10.1016/j.neulet.2011.05.054

Chen JL, Flanders GH, Lee W-CA, et al (2011b) Inhibitory Dendrite Dynamics as a General Feature of the Adult Cortical Microcircuit. J Neurosci 31:12437–12443. doi: 10.1523/JNEUROSCI.0420-11.2011

Chen JL, Lin WC, Cha JW, et al (2011c) Structural basis for the role of inhibition in facilitating adult brain plasticity. Nat Neurosci 14:587–94. doi: 10.1038/nn.2799

Chen JL, Nedivi E (2013) Highly Specific Structural Plasticity of Inhibitory Circuits in the Adult Neocortex. Neurosci 19:384–393. doi: 10.1177/1073858413479824

Chen JL, Villa KL, Cha JW, et al (2012) Clustered dynamics of inhibitory synapses and

dendritic spines in the adult neocortex. Neuron 74:361–73. doi: 10.1016/j.neuron.2012.02.030

Cohen-Cory S, Fraser SE (1995) Effects of brain-derived neurotrophic factor on optic axon branching and remodelling in vivo. Nature 378:192–196.

De Paola V, Holtmaat A, Knott G, et al (2006) Cell type-specific structural plasticity of axonal branches and boutons in the adult neocortex. Neuron 49:861–875. doi: 10.1016/j.neuron.2006.02.017

Du X, Hill RA (2015) 7,8-Dihydroxyflavone as a pro-neurotrophic treatment for neurodevelopmental disorders. Neurochem Int 89:170–180. doi: 10.1016/j.neuint.2015.07.021

Engert F, Bonhoeffer T (1999) Dendritic spine changes associated with hippocampal long-term synaptic plasticity. Nature 399:66–70. doi: 10.1038/19978

Escobar ML, Figueroa-Guzmán Y, Gómez-Palacio-Schjetnan A (2003) In vivo insular cortex LTP induced by brain-derived neurotrophic factor. Brain Res 991:274–279. doi: 10.1016/j.brainres.2003.08.015

Feng G, Mellor RH, Bernstein M, et al (2000) Imaging neuronal subsets in transgenic mice expressing multiple spectral variants of GFP. Neuron 28:41–51.

Granseth B, Fukushima Y, Sugo N, et al (2013) Regulation of thalamocortical axon branching by BDNF and synaptic vesicle cycling. Front Neural Circuits 7:202. doi: 10.3389/fncir.2013.00202

Grillo FW, Song S, Teles-Grilo Ruivo LM, et al (2013) Increased axonal bouton dynamics in the aging mouse cortex. Proc Natl Acad Sci 110:E1514–E1523. doi: 10.1073/pnas.1218731110

Grutzendler J, Kasthuri N, Gan WW-B (2002) Long-term dendritic spine stability in the adult cortex. Nature 420:812–816. doi: 10.1038/nature01151.1.

Guić-Robles E, Valdivieso C, Guajardo G (1989) Rats can learn a roughness discrimination using only their vibrissal system. Behav Brain Res 31:285–289. doi: 10.1016/0166-4328(89)90011-9

Hofer SB, Mrsic-Flogel TD, Bonhoeffer T, Hübener M (2009) Experience leaves a lasting structural trace in cortical circuits. Nature 457:313–317. doi: 10.1038/nature07487

Holtmaat A, Bonhoeffer T, Chow DK, et al (2009) Long-term, high-resolution imaging in the mouse neocortex through a chronic cranial window. Nat Protoc 4:1128–1144. doi: 10.1038/nprot.2009.89

Holtmaat A, Svoboda K (2009) Experience-dependent structural synaptic plasticity in the mammalian brain. Nat Rev Neurosci 10:647–58. doi: 10.1038/nrn2699

Holtmaat A, Wilbrecht L, Knott GW, et al (2006) Experience-dependent and cell-type-specific spine growth in the neocortex. Nature 441:979–983. doi: 10.1038/nature04783

Holtmaat AJGD, Trachtenberg JT, Wilbrecht L, et al (2005) Transient and persistent dendritic spines in the neocortex in vivo. Neuron 45:279–291. doi: 10.1016/j.neuron.2005.01.003

Hopkins ME, Bucci DJ (2010) BDNF expression in perirhinal cortex is associated with exercise-induced improvement in object recognition memory. Neurobiol Learn Mem 94:278–284. doi: 10.1016/j.nlm.2010.06.006

Jang S-W, Liu X, Yepes M, et al (2010) A selective TrkB agonist with potent neurotrophic activities by 7,8-dihydroxyflavone. Proc Natl Acad Sci U S A 107:2687–92. doi: 10.1073/pnas.0913572107

Kang H, Welcher AA, Shelton D, Schuman EM (1997) Neurotrophins and time: Different roles for TrkB signaling in hippocampal long-term potentiation. Neuron

19:653–664. doi: 10.1016/S0896-6273(00)80378-5

Keck T, Scheuss V, Jacobsen RI, et al (2011) Loss of sensory input causes rapid structural changes of inhibitory neurons in adult mouse visual cortex. Neuron 71:869–82. doi: 10.1016/j.neuron.2011.06.034

Knott GW, Holtmaat A, Wilbrecht L, et al (2006) Spine growth precedes synapse formation in the adult neocortex in vivo. Nat Neurosci 9:1117–1124. doi: 10.1038/nn1747

Leger M, Quiedeville A, Bouet V, et al (2013) Object recognition test in mice. Nat Protoc 8:2531–2537. doi: 10.1038/nprot.2013.155

Lom B, Cohen-Cory S (1999) Brain-Derived Neurotrophic Factor Differentially Regulates Retinal Ganglion Cell Dendritic and Axonal Arborization In Vivo. J Neurosci 19:9928–9938.

Lu B, Nagappan G, Guan X, et al (2013) BDNF-based synaptic repair as a disease-modifying strategy for neurodegenerative diseases. Nat Rev Neurosci 14:401–416. doi: 10.1038/nrn3505

Luo D, Shi Y, Wang J, et al (2016) 7,8-dihydroxyflavone protects 6-OHDA and MPTP induced dopaminergic neurons degeneration through activation of TrkB in rodents. Neurosci Lett 620:43–49. doi: 10.1016/j.neulet.2016.03.042

Matsuzaki M, Honkura N, Ellis-Davies GCR, Kasai H (2004) Structural basis of long-term potentiation in single dendritic spines. Nature 429:761–6. doi: 10.1038/nature02617

Miller MW, Pitts AF (2000) Neurotrophin receptors in the somatosensory cortex of the mature rat: Co-localization of p75, trk, isoforms and c-neu. Brain Res 852:355–366. doi: 10.1016/S0006-8993(99)02176-9

Minichiello L (2009) TrkB signalling pathways in LTP and learning. Nat Rev Neurosci

10:850–60. doi: 10.1038/nrn2738

Minichiello L, Calella AM, Medina DL, et al (2002) Mechanism of TrkB-mediated hippocampal long-term potentiation. Neuron 36:121–137. doi: 10.1016/S0896-6273(02)00942-X

Nagahara AH, Tuszynski MH (2011) Potential therapeutic uses of BDNF in neurological and psychiatric disorders. Nat Rev Drug Discov 10:209–219. doi: 10.1038/nrd3366

Pandya CD, Kutiyanawalla A, Pillai A (2013) BDNF-TrkB signaling and neuroprotection in schizophrenia. Asian J Psychiatr 6:22–28. doi: 10.1016/j.ajp.2012.08.010

Porrero C, Rubio-Garrido P, Avendaño C, Clascá F (2010) Mapping of fluorescent protein-expressing neurons and axon pathways in adult and developing Thy1-eYFP-H transgenic mice. Brain Res 1345:59–72. doi: 10.1016/j.brainres.2010.05.061

Simon P, Dupuis R, Costentin J (1994) Thigmotaxis as an index of anxiety in mice. Influence of dopaminergic transmissions. Behav Brain Res 61:59–64.

Svoboda K, Tank DW, Denk W (1996) Direct Measurement of Coupling Between Dendritic Spines and Shafts. Science (80-) 272:716–719. doi: 10.1126/science.272.5262.716

Trachtenberg JT, Chen BE, Knott GW, et al (2002) Long-term in vivo imaging of experience-dependent synaptic plasticity in adult cortex. Nature 420:788–94. doi: 10.1038/nature01273

Tyler WJ, Pozzo-Miller L (2003) Miniature synaptic transmission and BDNF modulate dendritic spine growth and form in rat CA1 neurones. J Physiol 553:497–509. doi: 10.1113/jphysiol.2003.052639

Uluc K, Kendigelen P, Fidan E, et al (2013) TrkB receptor agonist 7, 8 dihydroxyflavone

triggers profound gender- dependent neuroprotection in mice after perinatal hypoxia and ischemia. CNS Neurol Disord Drug Targets 12:360–70. doi: CDTCNSND-EPUB-20130227-13 [pii]

van Versendaal D, Rajendran R, Saiepour MH, et al (2012) Elimination of inhibitory synapses is a major component of adult ocular dominance plasticity. Neuron 74:374–83. doi: 10.1016/j.neuron.2012.03.015

von Heimendahl M, Itskov PM, Arabzadeh E, Diamond ME (2007) Neuronal Activity in Rat Barrel Cortex Underlying Texture Discrimination. PLoS Biol 5:e305. doi: 10.1371/journal.pbio.0050305

Yang YJ, Li YK, Wang W, et al (2014) Small-molecule TrkB agonist 7,8-dihydroxyflavone reverses cognitive and synaptic plasticity deficits in a rat model of schizophrenia. Pharmacol Biochem Behav 122:30–36. doi: 10.1016/j.pbb.2014.03.013

Yoshii A, Constantine-Paton M (2010) Postsynaptic BDNF-TrkB signaling in synapse maturation, plasticity, and disease. Dev Neurobiol 70:304–22. doi: 10.1002/dneu.20765

Zeng Y, Liu Y, Wu M, et al (2012a) Activation of TrkB by 7,8-dihydroxyflavone prevents fear memory defects and facilitates amygdalar synaptic plasticity in aging. J Alzheimer's Dis 31:765–778. doi: 10.3233/JAD-2012-120886

Zeng Y, Lv F, Li L, et al (2012b) 7,8-Dihydroxyflavone Rescues Spatial Memory and Synaptic Plasticity in Cognitively Impaired Aged Rats. J Neurochem 122:800–811. doi: 10.1111/j.1471-4159.2012.07830.x

Zhang J, Wu J, Fujita Y, et al (2015) Antidepressant effects of TrkB ligands on depression-like behavior and dendritic changes in mice after inflammation. Int J Neuropsychopharmacol 18:1–12. doi: 10.1093/ijnp/pyu077

1 Zhang MW, Zhang S feng, Li ZH, Han F (2016) 7,8-Dihydroxyflavone reverses the
2 depressive symptoms in mouse chronic mild stress. Neurosci Lett 635:33–38. doi:
3 10.1016/j.neulet.2016.10.035

4 Zhang Z, Liu X, Schroeder JP, et al (2014) 7,8-Dihydroxyflavone Prevents Synaptic
5 Loss and Memory Deficits in a Mouse Model of Alzheimer's Disease.
6 Neuropsychopharmacology 39:638–650. doi: 10.1038/npp.2013.243

7 Zuccato C, Cattaneo E (2009) Brain-derived neurotrophic factor in neurodegenerative
8 diseases. Nat Rev Neurol 5:311–322. doi: 10.1038/nrneurol.2009.54

9

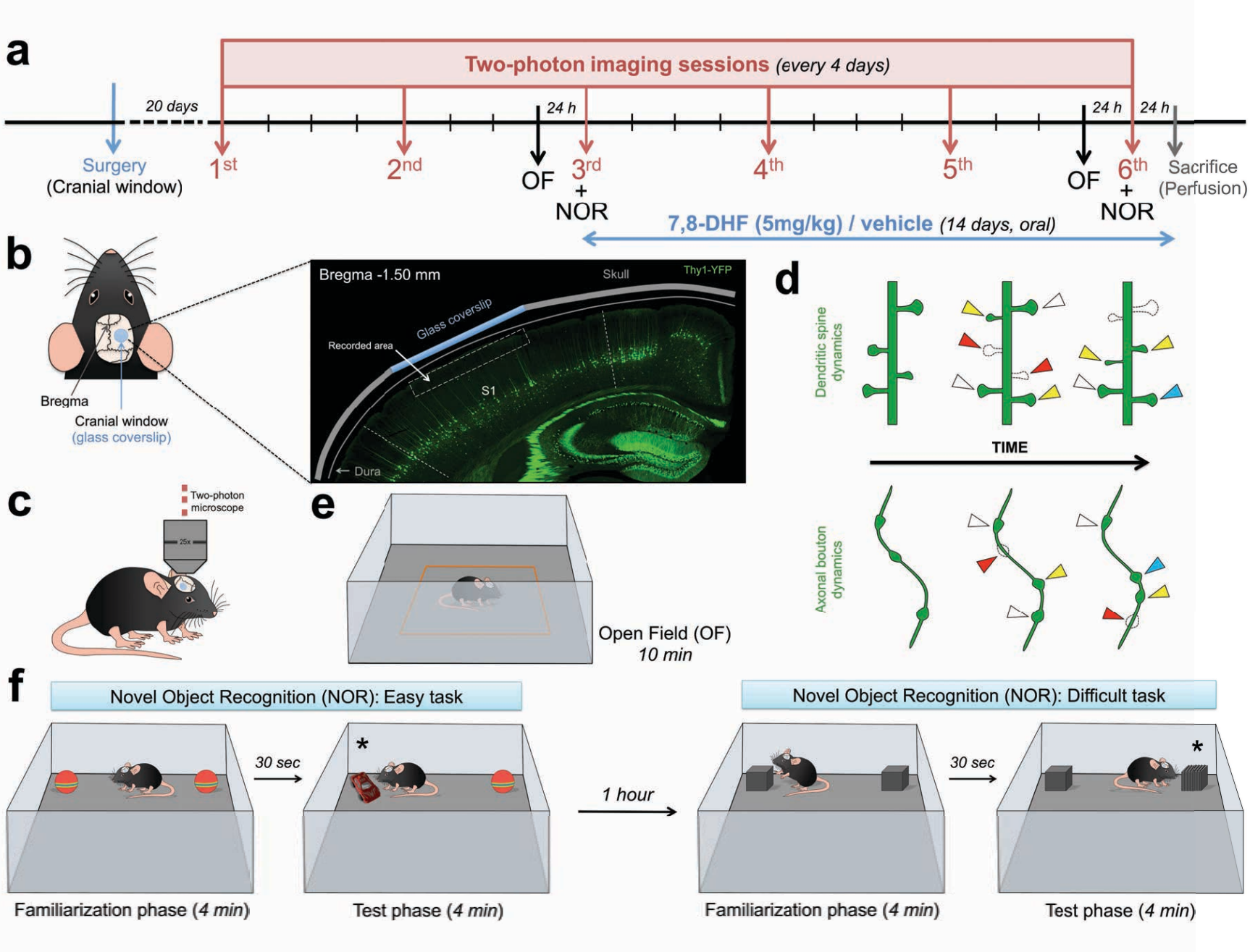
a
Two-photon imaging sessions (every 4 days)
20 days
24 h
24 h
24 h
Surgery
(Cranial window)
1st
2nd
OF
3rd
+
NOR
4th
5th
OF
6th
+
NOR
Sacrifice
(Perfusion)
7,8-DHF (5mg/kg) / vehicle (14 days, oral)
b
Bregma
Cranial window
(glass coverslip)
Bregma -1.50 mm
Skull
Thy1-YFP
Glass coverslip
Recorded area
S1
Dura
c
Two-photon
microscope
25x
d
Dendritic spine
dynamics
TIME
Axonal bouton
dynamics
e
Open Field (OF)
10 min
f
Novel Object Recognition (NOR): Easy task
30 sec
*
Familiarization phase (4 min)
Test phase (4 min)
1 hour
Novel Object Recognition (NOR): Difficult task
30 sec
*
Familiarization phase (4 min)
Test phase (4 min)

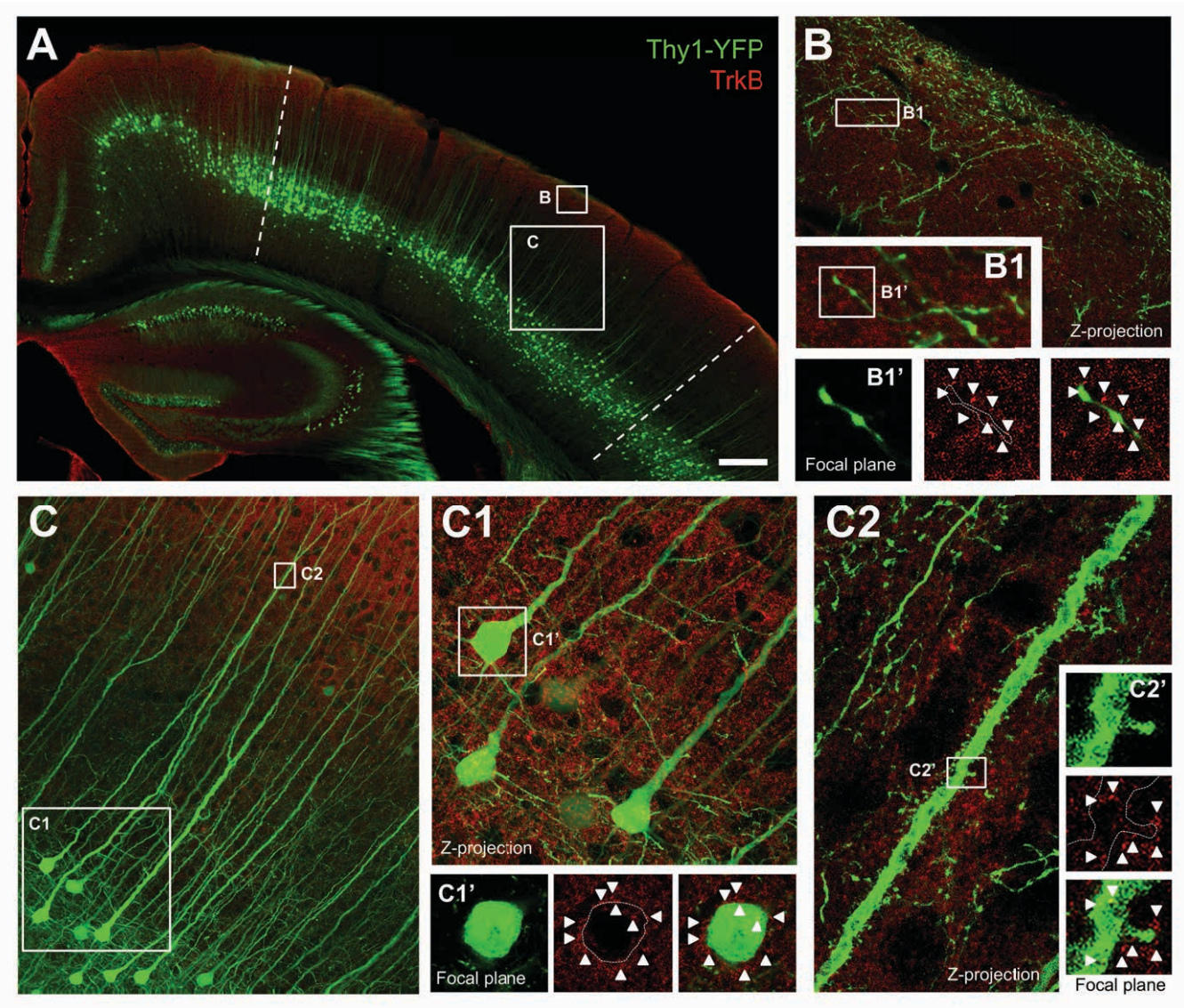
A
Thy1-YFP
TrkB
B
C
B
B1
B1
B1'
Z-projection
B1'
Focal plane
C
C2
C1
C1
C1'
Z-projection
C1'
Focal plane
C2
C2'
C2'
Z-projection
C2'
Focal plane

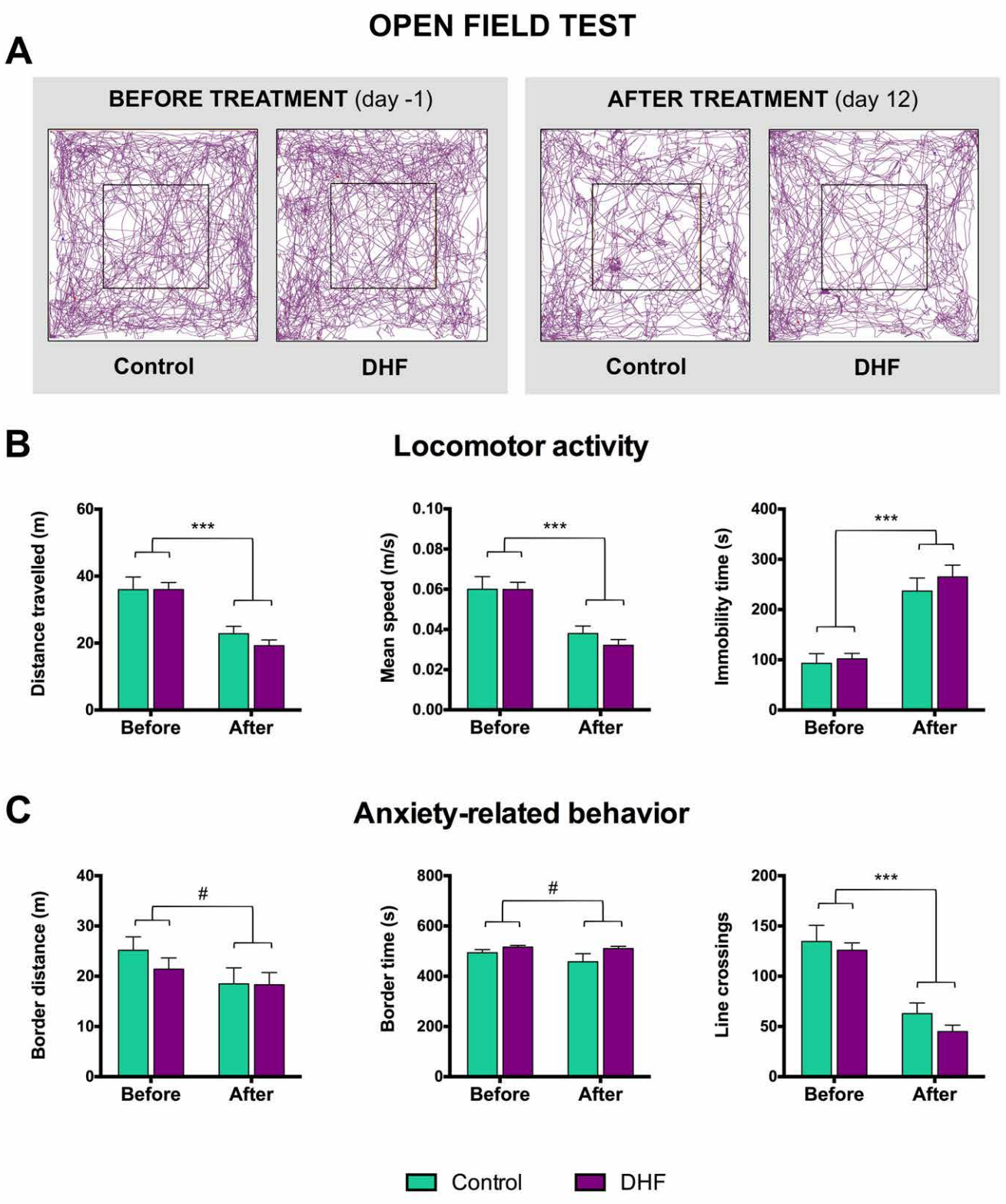
OPEN FIELD TEST
A
BEFORE TREATMENT (day -1)
AFTER TREATMENT (day 12)
Control
DHF
Control
DHF
B
Locomotor activity
Distance travelled (m)
Mean speed (m/s)
Immobility time (s)
Before
After
C
Anxiety-related behavior
Border distance (m)
Border time (s)
Line crossings
Control
DHF

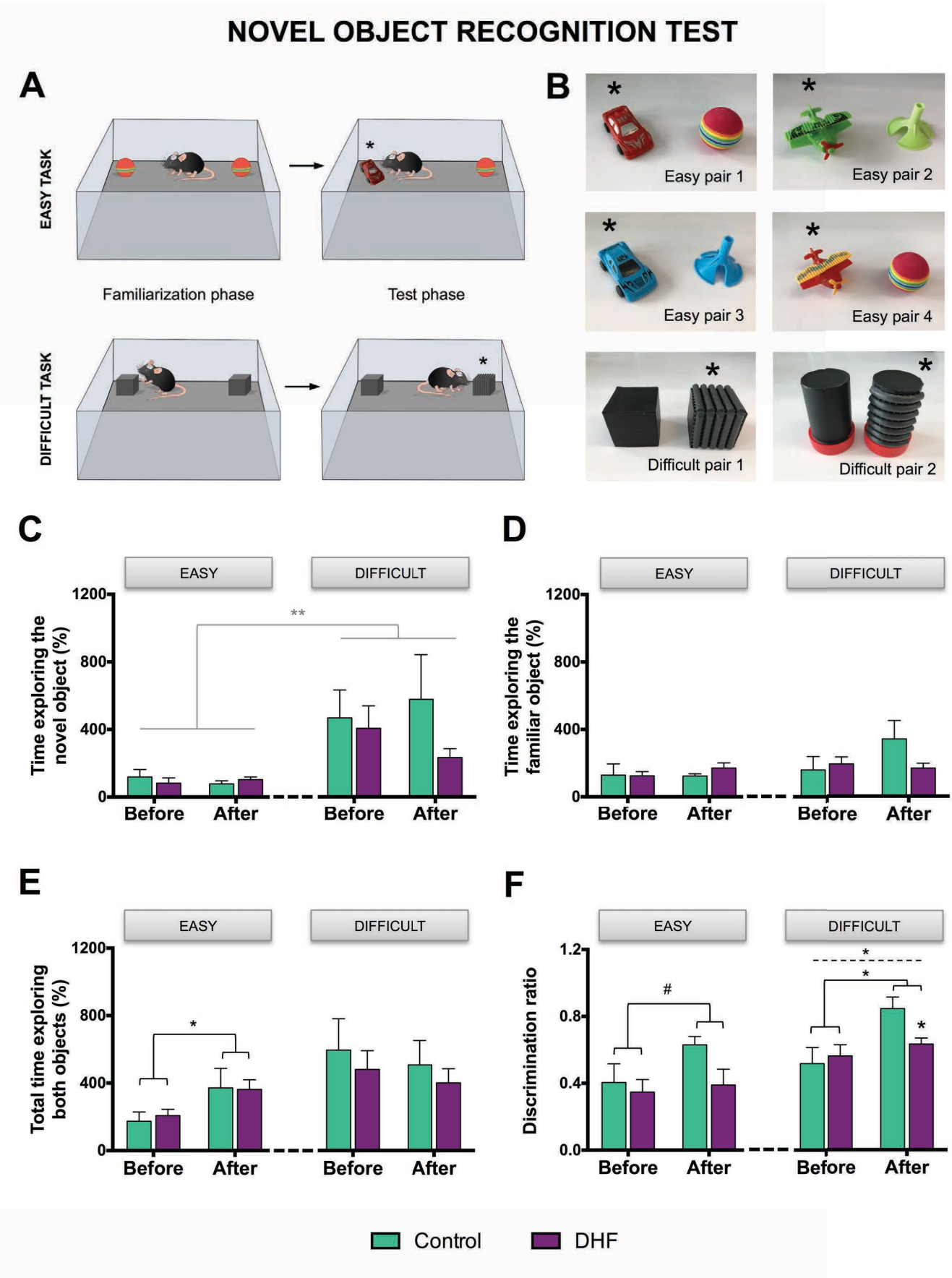
NOVEL OBJECT RECOGNITION TEST
A
EASY TASK
Familiarization phase
Test phase
DIFFICULT TASK
B
Easy pair 1
Easy pair 2
Easy pair 3
Easy pair 4
Difficult pair 1
Difficult pair 2
C
EASY
DIFFICULT
Time exploring the novel object (%)
1200
800
400
0
**
Before
After
Before
After
D
Time exploring the familiar object (%)
E
Total time exploring both objects (%)
*
F
Discrimination ratio
1.2
0.8
0.4
0.0
#
Control
DHF

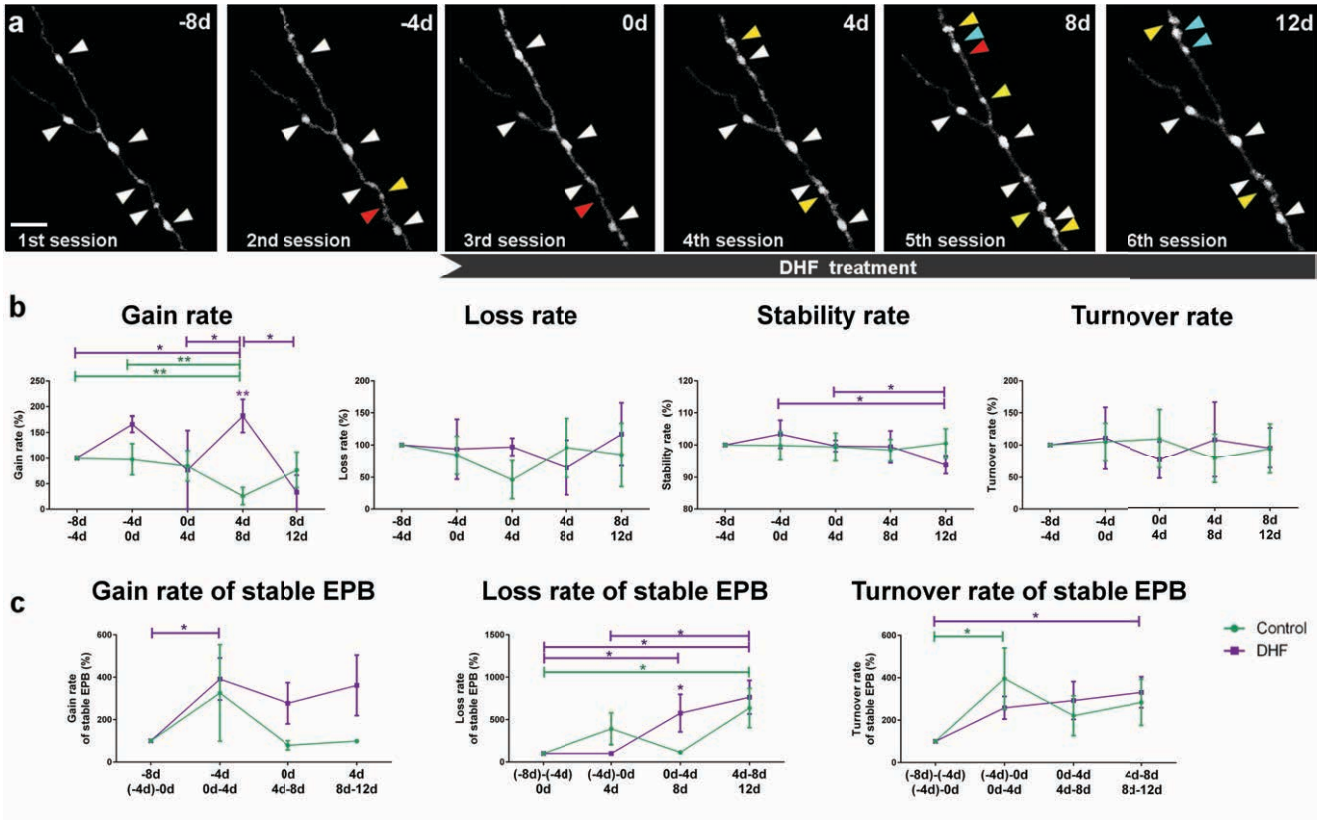
a
-8d
-4d
0d
4d
8d
12d
1st session
2nd session
3rd session
4th session
5th session
6th session
DHF treatment
b
Gain rate
Loss rate
Stability rate
Turnover rate
Gain rate (%)
Loss rate (%)
Stability rate (%)
Turnover rate (%)
-8d -4d
-4d 0d
0d 4d
4d 8d
8d 12d
c
Gain rate of stable EPB
Loss rate of stable EPB
Turnover rate of stable EPB
Gain rate of stable EPB (%)
Loss rate of stable EPB (%)
Turnover rate of stable EPB (%)
(-8d)-(-4d) 0d
(-4d)-0d 4d
0d-4d 8d
4d-8d 12d
-8d (-4d)-0d
-4d 0d-4d
0d 4d-8d
4d 8d-12d
Control
DHF

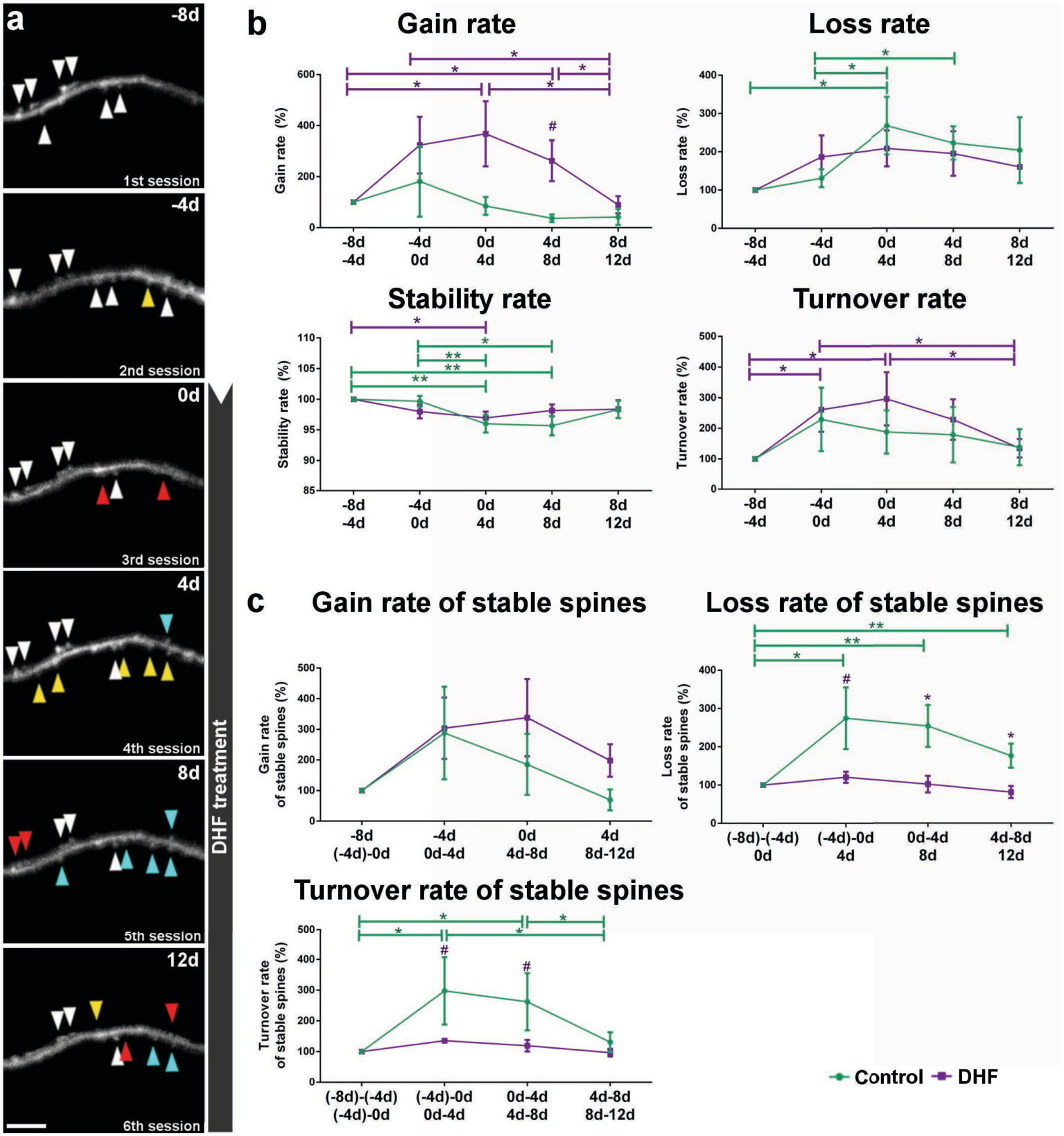
a
-8d
1st session
-4d
2nd session
0d
3rd session
4d
4th session
8d
5th session
12d
6th session
DHF treatment
b
Gain rate
Gain rate (%)
Loss rate
Loss rate (%)
Stability rate
Stability rate (%)
Turnover rate
Turnover rate (%)
-8d -4d
-4d 0d
0d 4d
4d 8d
8d 12d
c
Gain rate of stable spines
Gain rate of stable spines (%)
Loss rate of stable spines
Loss rate of stable spines (%)
Turnover rate of stable spines
Turnover rate of stable spines (%)
-8d (-4d)-0d
-4d 0d-4d
0d 4d-8d
4d 8d-12d
(-8d)-(-4d) 0d
(-4d)-0d 4d
0d-4d 8d
4d-8d 12d
(-8d)-(-4d) (-4d)-0d
(-4d)-0d 0d-4d
0d-4d 4d-8d
4d-8d 8d-12d
Control
DHF

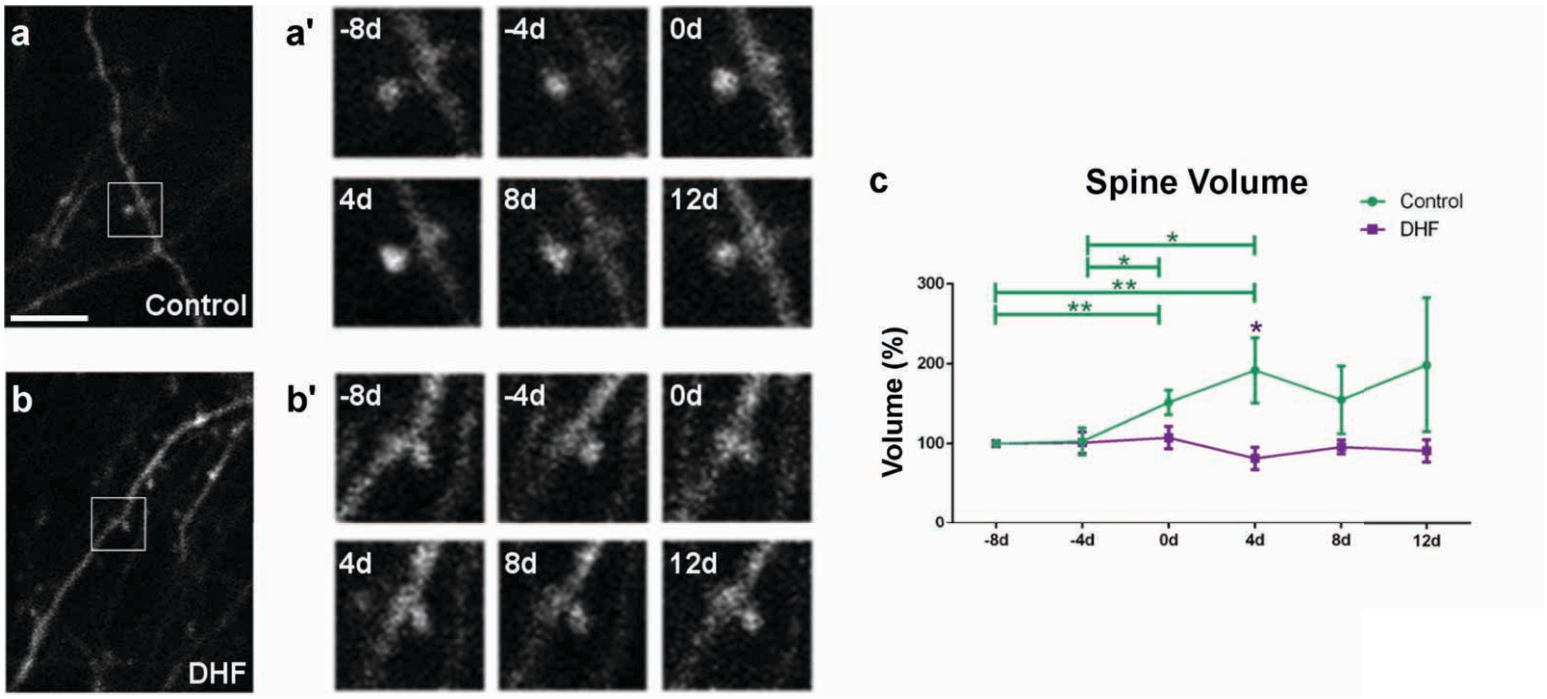
a
Control
a'
-8d
-4d
0d
4d
8d
12d
b
DHF
b'
-8d
-4d
0d
4d
8d
12d
c
Spine Volume
Control
DHF
Volume (%)
300
200
100
0
*
*
**
**
*
-8d
-4d
0d
4d
8d
12d

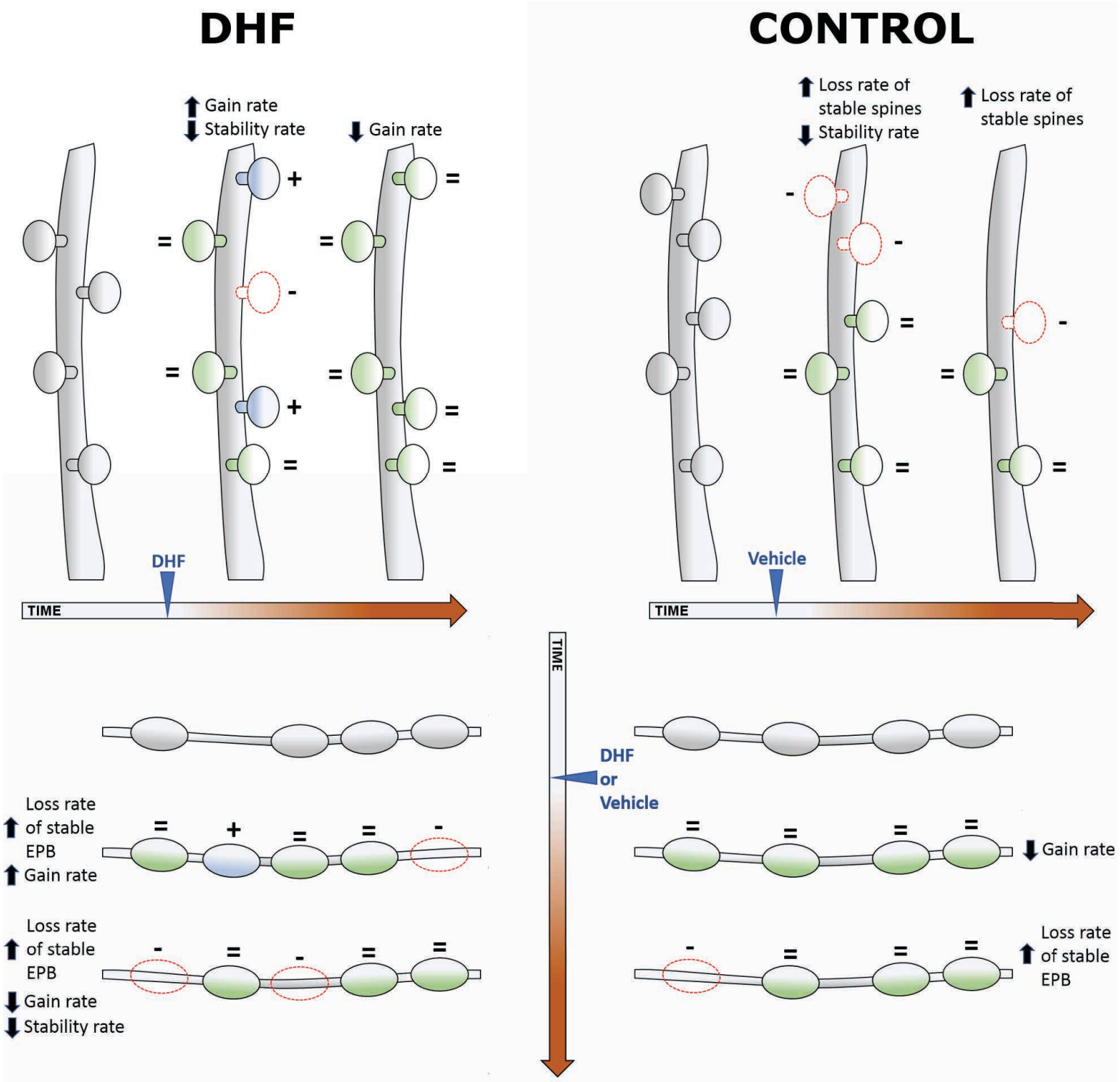
DHF
CONTROL
Gain rate
Stability rate
Gain rate
Loss rate of stable spines
Stability rate
Loss rate of stable spines
DHF
Vehicle
TIME
TIME
TIME
DHF or Vehicle
Loss rate of stable EPB
Gain rate
Loss rate of stable EPB
Gain rate
Stability rate
Gain rate
Loss rate of stable EPB

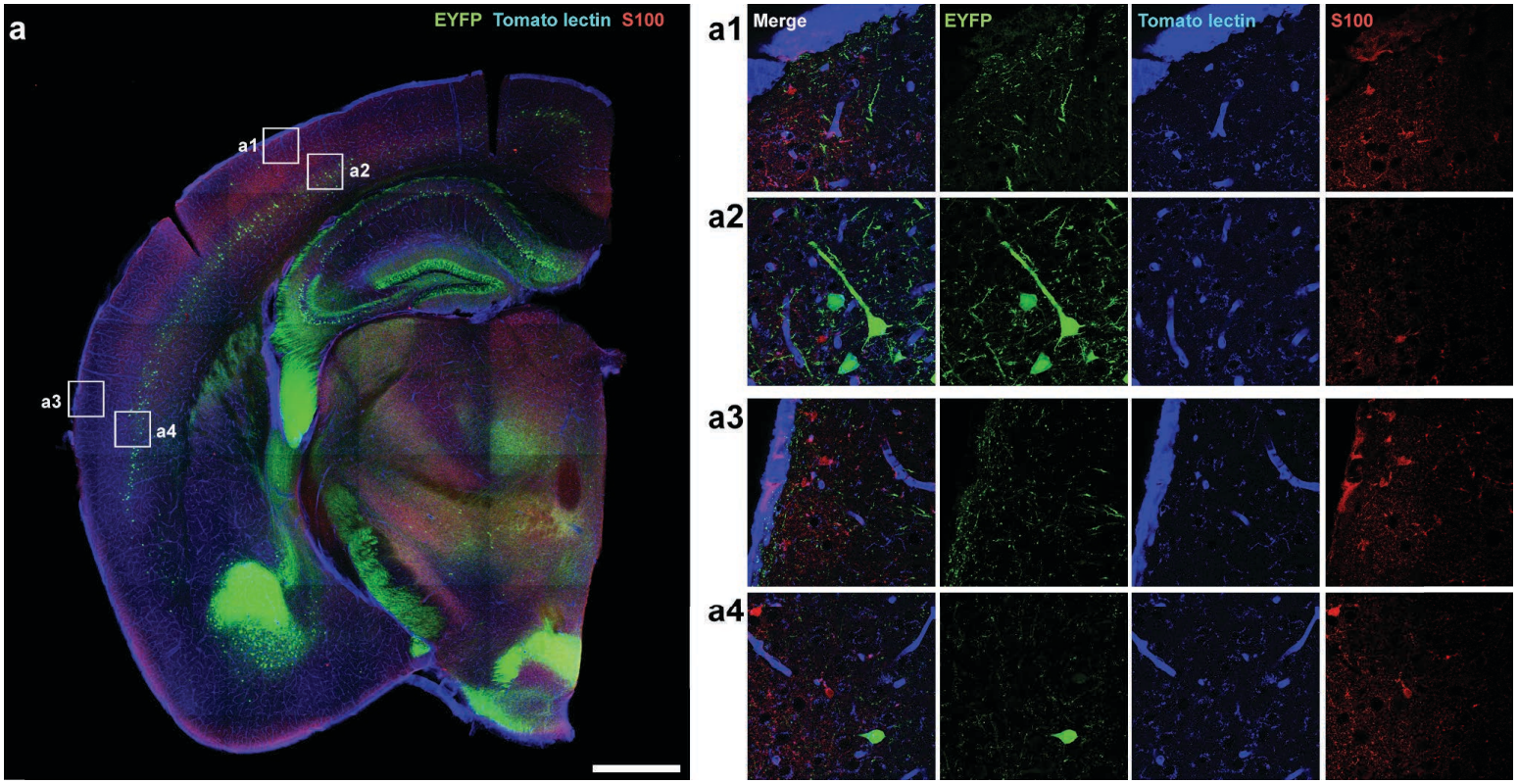
a
EYFP Tomato lectin S100
a1
a2
a3
a4
a1
Merge
EYFP
Tomato lectin
S100
a2
a3
a4